Journal of Cleaner Production 486 (2025) 144428

Contents lists available at ScienceDirect

Journal of Cleaner Production

journal homepage: www.elsevier.com/locate/jclepro

CO_2 adsorption on cellulose nanofiber-polyethyleneimine functionalized membranes

Gabriela A. Bastida [a,b], Roberto J. Aguado [a,*], Marc Delgado-Aguilar [a], Miguel A. Zanuttini [b], María V. Galván [b], Quim Tarrés [a]

[a] LEPAMAP-PRODIS Research Group, University of Girona, C. Maria Aurèlia Capmany 61, 17003, Girona, Spain
[b] Instituto de Tecnología Celulósica, Facultad de Ingeniería Química (FIQ-CONICET), Universidad Nacional del Litoral, Santiago del Estero, 2654, S3000AOJ, Santa Fe, Argentina

ARTICLE INFO

Handling Editor: Yutao Wang

Keywords:
CO_2 capture
Polyethyleneimine
Membrane
Nanocellulose
Sustainable materials

ABSTRACT

This research addresses two limitations of electrospun membranes consisting of cellulose acetate (CA) and polyethylenimine (PEI) for CO_2 capture. Such setbacks are the easy elution of PEI from the CA matrix in the presence of water and their relatively poor mechanical properties. The approach involves the innovative incorporation of oxalic acid-treated cellulose nanofibers (CNF) to increase PEI retention, besides burst and tensile strength. The synergistic effects of CNF and PEI, based on ammonium carboxylate formation, are postulated to enhance CO_2 uptake. The study evaluates the adsorption capacity of 14 different membranes, analyzing their physical, mechanical, and chemical properties. It also implies the optimization of the PEI content to prevent elution and ensure proper performance for potential off-gas treatments. In this context, esterification with oxalic acid was deemed a more suitable method to introduce carboxyl groups on cellulose than the well-known TEMPO-mediated oxidation, since the latter resulted in highly viscous CNF suspensions, unfit for electrospinning. Overall, the best performance was attained by membranes containing 4 wt% PEI and CNF pretreated with 75 wt % oxalic acid. CO_2 adsorption followed pseudo-first order kinetics, reaching saturation values over 4 mmol/g. Moreover, membranes were reusable, not detecting any significant loss in adsorption capacity along five cycles. All considered, this study proposes a robust solution for sustainable industrial processes, both in terms of resisting stress and in terms of CO_2 capture.

1. Introduction

The development of efficient carbon dioxide (CO_2) adsorption membranes is a promising avenue for mitigating CO_2 emissions. Among CO_2 separation methods, membrane separation stands out for its low energy consumption, cost-effectiveness, compact design, environmental friendliness, and straightforward operation (Jang et al., 2022; Vakharia et al., 2018). Furthermore, there is a growing need to use environmentally sustainable materials and fabrication techniques. Integrating membranes produced in environmentally friendly ways with the existing CO_2 capture infrastructure present significant challenges.

In membrane manufacturing, cellulose acetate (CA) is commonly used due to its ability to form dense, asymmetric, and/or porous membranes through processes like phase inversion or electrospinning (Luo et al., 2022). Electrospinning involves applying high voltage to a polymer solution to create nanofilaments that are collected to form a membrane (Xue et al., 2019). These membranes are widely used in water treatment (Li et al., 2022), biosensing (Chauhan and Solanki, 2019), and biomedical fields (Dos Santos et al., 2020). Nonetheless, CA lacks any particular affinity for CO_2.

Conversely, polyethyleneimine (PEI) exhibits good CO_2 adsorption potential but lacks membrane-forming properties. Bridging this gap requires innovative approaches to integrate the strengths of both materials. PEI consists of linear or branched chains of repeating $–CH_2CH_2NH–$ units (Payne et al., 2020). Its high density of amine groups makes PEI a potent proton acceptor, allowing it to effectively capture and bind acidic species in solution or gas phase (Liu et al., 2022). The amino groups in PEI can react reversibly with CO_2 (Meng et al., 2021), although stable

Abbreviations: BEP, bleached eucalyptus pulp; CA, cellulose acetate; CMFN, cellulose micro/nanofiber; CNF, cellulose nanofibers; PEI, polyethyleneimine; TEMPO, 2,2,6,6-Tetramethylpiperidine 1-oxyl.

* Corresponding author.
E-mail address: roberto.aguado@udg.edu (R.J. Aguado).

https://doi.org/10.1016/j.jclepro.2024.144428
Received 15 July 2024; Received in revised form 6 November 2024; Accepted 6 December 2024
Available online 11 December 2024

carbamate bond formation is less likely due to the relatively low mobility of polymer chains.

In a recent study, Yoon et al. (2024) fabricated electrospun cellulose acetate (CA) filaments with a high concentration of PEI, effectively capturing carbon dioxide through physisorption. Remarkably, the CO_2 adsorption capacity remained at 99% even after five adsorption-desorption cycles. Despite their success, they did not test the quality of the attachment of PEI to CA or the moisture resistance of the membranes. Regarding the relevance of PEI's hydrophilic character, Hou et al. (2016) had previously quantified the extent of swelling and the loss of PEI following immersion of CA/PEI in water. They attained high retention of PEI as long as its concentration was low, but increasing PEI content raised the electrostatic repulsion among lateral polar groups, causing notorious amounts of PEI to diffuse outwards. Given that water vapor is produced in most combustion processes, preventing the elution of PEI chains by water molecules would enhance the potential of CA/PEI systems for CO_2 capture.

The hypothesis driving the present study is that integrating CA/PEI electrospun materials with negatively-charged cellulose nanofibers (CNF) introduces a two-pronged improvement, reinforcing the membrane structure and promoting ionic bonding with PEI. Out of the diverse methods leading to cellulosic materials with anionic functional groups, esterification with oxalic acid is compared to TEMPO-mediated oxidation. We assessed the interplay between CA, PEI, and CNF, aiming at producing membranes able to withstand multiple cycles of adsorption and desorption without significant degradation. The CO_2 adsorption capacity of 14 types of membranes was examined, providing a comprehensive evaluation of their physical and chemical properties. Besides, this study optimized the amount of PEI to ensure it does not elute from the membrane, which would compromise its performance as adsorbent. The membranes exhibiting the most promising attributes underwent further investigation to evaluate their reusability.

2. Material and methods

2.1. Production of cellulose micro/nanofibers

Cellulose micro/nanofibers (CMNF) were produced using bleached eucalyptus pulp (BEP) (DP_w of 7750) provided by Suzano Papel e Celulose S.A. (Aracruz, Brazil). The pulp underwent an initial mechanical pretreatment in a PFI mill refiner, with 10,000 revolutions. Subsequently, a chemical pretreatment with oxalic acid at three concentration levels (25, 50, and 75 wt%) was performed for 1 h at 90 °C, under overhead stirring at 250 rpm (Bastida et al., 2022). For the obtention of CMNF without oxalic acid reaction, BEP was pretreated in a PFI mill at 20,000 revolutions.

For comparison purposes with more conventional approaches for the chemical modification before homogenization, CNF_{T3} were produced in parallel by TEMPO-mediated oxidation. This reaction was performed at pH 10 with a consistency of 1 wt% according to Serra et al. (2017). Specifically, the dosage of spent oxidizer (NaClO) was 3 mmol per gram of oven-dried pulp.

All pretreated pulps were thoroughly washed with distilled water and filtered. All 1 wt% suspensions were homogenized first at 300 bar, then at 600 bar, and finally at 900 bar, each for three passes. The different samples of micro/nanofibrillated cellulose obtained this way were labeled in regard to the oxalic acid concentration used in the chemical pretreatment: $CMNF_0$, $CMNF_{25}$, $CMNF_{50}$, and $CMNF_{75}$.

2.2. Preparation of electrospinning solutions

Due to the setbacks implied by micro-sized fibers in electrospinning (Bastida et al., 2024), the nanofraction of CMNF samples was first isolated. This was attained by centrifugation at 3800*g* for 20 min, discarding the settled part. The colloidal dispersion obtained corresponded to CNF of different kinds, as a function of the oxalic acid concentration: CNF_0, CNF_{25}, CNF_{50}, and CNF_{75}.

A homogeneous electrospinning solution containing 10 wt% CA was prepared using a ternary solvent system of acetone/DMF/water in a ratio of 3:2:1 (Chen et al., 2020). The mixture was stirred for 6 h at 25 °C to ensure the complete dissolution of CA. Different formulations were then created by replacing the water volume with a 6 wt% suspension of each type of CNF, as determined to be optimal in a previous study (Bastida et al., 2024), along with varying amounts of PEI.

2.3. Preparation and characterization of CA, CA−PEI, and CA−CNF_x−PEI membranes

Membranes were produced following the procedure outlined by Chen et al. (2020) using an electrospinning setup (Fuidnatek, Bionicia, Paterna, Spain) equipped with a 20-gauge needle tip (nominal outer diameter: 0.908 mm). The feed rate was set to 35 μL/min, an applied voltage of 16 kV was used, and a receiving distance of 5 cm was maintained between the needle tip and the aluminum foil collector. The electrospinning chamber was at 23 °C and its initial relative humidity (RH) was 50%.

The resulting membranes were then air-dried. To distinguish between free PEI and attached PEI, membranes were washed for 30 min in a 0.02N NaOH solution, rinsed with distilled water, and then analyzed both with and without washing. The designations of the 19 membranes are listed in Table S1. For them to be comparable to each other, the membranes were conditioned at 23 ± 1 °C and a RH of 50% for 48 h before testing. Each sample was analyzed in triplicate, and the results were averaged.

The grammage of the membranes was determined by the weight to surface area ratio. Density was determined using the membrane's dimensions and weight. Volume was calculated based on the thickness, which was measured using a digital micrometer from Starrett (Athol, MA, USA). The percentage of void volume, was calculated from Eq. (1):

$$\text{Void volume}\ (\%) = \left(1 - \frac{\rho_m}{\rho_{CA}}\right) * 100 \quad (1)$$

where ρ_m and ρ_{CA} are the different membranes and the cellulose acetate density, respectively. Morphological characteristics were observed by Scanning Electronic Microscopy (SEM) (TESCAN Clara, Brno, Czech Republic). Images were captured using ultra-high resolution (UH−resolution) at an accelerating voltage of 1 kV. Samples were prepared for analysis by affixing them to a sample holder with conductive carbon tape and coating them with a thin layer of carbon using an Emitech K950 turbo evaporator device. Elemental analysis and sample mapping were conducted using Energy Dispersive Spectroscopy (EDS) integrated with the SEM. SEM images were processed using the open-source software ImageJ to measure pore sizes, following the method reported by Hojat et al. (2023).

Tensile tests were carried out using an INSTRON 3340 testing machine with a 100 N load cell. Measurements were performed on strips with dimensions of 15 mm width and 80 mm length at a crosshead speed of 5 mm/min. The burst strength (Mullen Index) was tested under ISO 2758.

2.4. Assessment of CO_2 adsorption capacity

The influence of different CNF characteristics and PEI amount on CO_2 membrane adsorption capability was examined. Membranes was subjected to a continuous flow operation at a rate of 1 Nl/min CO_2. CO_2 retention was assessed every 2 min until constant adsorption to establish kinetics. CO_2 was desorbed of membrane in 50 mL of a 0.02N NaOH solution over 30 min (Fig. S1). Subsequently, a titration with 0.01N HCl at two equivalence points is carried out, followed by precipitation of $BaCO_3$ using a 0.01N $BaCl_2$ solution. These two methods were employed to corroborate the results. From the point where an accurate

determination of the weight of the precipitate was possible, the values obtained from both methods agreed. The top-performing membranes were tested to determine the number of adsorption-desorption cycles they could endure without compromising their properties.

All membranes were analyzed using Fourier transform infrared spectroscopy (FTIR) before and after CO_2 adsorption. Spectra were collected on a Bruker Alpha FT-IR spectrometer equipped with a diamond crystal plate ATR single-reflection accessory, at a resolution of 4 cm^{-1} from 500 to 4000 cm^{-1}.

2.5. Additional characterizations

Detailed descriptions of the characterization methods of cellulose micro/nanofibers, cellulose nanofibers, and electrospinning solutions are provided in the Supplementary Information.

3. Results and discussion

3.1. Properties of nanocellulose suspensions

Table 1 evidences consistent trends in performance, electrical charge, and transmittance with the concentration of oxalic acid. It is observed that more aggressive pretreatments yielded a higher nanofraction, increasing both the charge and transparency of the nanofibers. This also affects the viscosity of the solutions, as the nanofraction exhibits strong effects as rheology modifier (Liao et al., 2021).

Likewise, the carboxyl group content increased with treatment intensity. Notably, at 75% oxalic acid ($CMNF_{75}$), the carboxyl group content exceeds that of cellulose nanofibers oxidized with 3 mmol/g of sodium hypochlorite (CNF_{T3}). Consequently, the cationic demand also increased with oxalic acid concentration. However, it is important to note that in this regard, due to the different specific surface area (Espinosa et al., 2020), the cationic demand was lower than that of TEMPO-oxidized nanofibers. This suggests that these oxalic acid-treated nanofibers are thicker than those oxidized by TEMPO, as hinted by the nanofibrillation yield, zeta potential, and transmittance (Delgado-Aguilar et al., 2015; Signori-Iamin et al., 2023). This has been directly confirmed by transmission electron microscopy in a previous work (Bastida et al., 2022). This feature is particularly interesting for preparing CO_2 adsorption membranes, aiming at a relatively high presence of carboxyl groups without excessively increasing the specific surface area of the nanofibers, which would otherwise enhance their water retention capacity.

The electrospinning process and the morphology of the resulting filaments depend on the operating parameters and the solutions used (Deitzel et al., 2001). Keeping operating parameters constant, it is imperative to examine those related to the system since these are essential to achieving adequate flow rate and jet stability, critical for a successful electrospinning process. As it known, viscosity and conductivity are strongly influenced by the type of nanofibers and PEI present in the electrospinning solution. Therefore, it is essential to find an optimal balance to achieve homogeneous solutions and ensure successful spinnability. However, this could not be achieved with all tested solutions. In the case of CNF_{T3}, due to its very high viscosity, it was difficult to pass the solution through the needle, causing blockages and an inconsistent flow rate that generated drops. On the other hand, the presence of microfraction in $CMNF_{50}$ caused needle blockages (Fig. 1). In the electrospinning configuration, a viscosity limit of 2 Pa s was experimentally established, below which membrane production is feasible. During the tests, it was observed that when the solution's viscosity did not exceed this limit, the flow remained continuous, splashing was absent, and the needle did not clog. However, for more viscous solutions, these issues did occur.

On the other hand, the suspension's higher conductivity will favor the continuous formation of filaments. The solution's conductivity is crucial in evenly distributing the electrical charge, thereby impacting Taylor cone formation at the needle tip during the electrospinning process (Morais et al., 2022; Xue et al., 2019). In essence, what is sought is an optimal balance of these two properties.

As shown in Fig. 1, suspensions of CA, CA with PEI, and cellulose acetate with non-pretreated nanofibers have relatively low viscosities compared to the established threshold for membrane production that allows continuous spinning without needle blockages. However, adding PEI or CNF increases the viscosity, with a more pronounced effect when both PEI and CNF are added. Indeed, the high viscosity of CNF suspensions presents challenges in achieving adequate flow rate and jet stability, vital for a successful electrospinning process.

The conductivity of the suspension also increased with the addition of PEI and CNF due to their higher electrostatic charge. With PEI exhibiting a measured conductivity of 360 μS/cm and CNF_x ranging from 60 to 80 μS/cm, the solutions were expected to demonstrate notable increases in electrical conductance. This increase in viscosity and conductivity was more significant when using CNF obtained with oxalic acid pretreatment, and it intensifies with the strength of the pretreatment. For instance, CNF_{75} reached an apparent viscosity slightly above 2 Pa, establishing this concentration of oxalic acid as the limit for obtaining CNF suitable for membrane production. For comparison, a suspension was characterized using both micro/nanofiber and nanofiber fractions obtained with 50% oxalic acid. The CA−$CMNF_{50}$ suspension, despite not exhibiting significantly different conductivity values from CA−CNF_{50}, showed notable thickening, thus limiting its applicability.

Suspensions formulated with nanofibers obtained through TEMPO oxidation resulted in viscosity values well above the limiting threshold, rendering them unsuitable for application. The gel−like consistency of these types of nanofibers created heterogeneity in the suspension, leading to conglomerations that ultimately blocked the needle. However, their conductivity values were similar to those obtained with the 75% oxalic acid CNF suspensions. This highlights the CNF treated with 75% oxalic acid as having the best ratio of surface charge to size, making them the most favorable for use in membrane production by electrospinning.

3.2. Membrane quality

The physicomechanical properties of the membranes electrospun from the suitable suspensions shown in Fig. 1 are presented in Table 2. The thickness of the CA reference membrane had a value of approximately 71 μm. Incorporating CNF without any pretreatment thickened the membranes, but the presence of PEI thinned them.

The analysis of the density data reveals several important trends. The addition of PEI to pure CA membranes resulted in a slight reduction in density. Incorporating CNF without pretreatment significantly lowered

Table 1
Effect of different pretreatments on nanofibers characteristics and viscosity solutions.

$CMNF_x$	Nanofibrillation yield (%)	Carboxylic content (μeq/g)	Cationic demand (eq/g)	ζ−potential (mV)	Transmittance (%)	Viscosity (mPa·s)
$CMNF_0$	12.6 ± 1.8	47.0 ± 5.2	264 ± 19	~0	7.3 ± 0.1	70.7 ± 12.1
$CMNF_{25}$	47.5 ± 0.3	373.5 ± 11.7	251 ± 14	−29.6 ± 0.2	35.4 ± 0.1	47.98 ± 9.8
$CMNF_{50}$	79.5 ± 0.7	455.9 ± 16.3	767 ± 23	−34.6 ± 0.1	73.8 ± 0.2	131.1 ± 23.7
$CMNF_{75}$	81.1 ± 1.2	907.9 ± 14.2	962 ± 14	−45.5 ± 0.4	84.2 ± 0.8	140.8 ± 17.6
CNF_{T3}	>95	513.6 ± 23.7	1328 ± 74	−48.3 ± 0.1	87.3 ± 0.1	145.6 ± 10.2

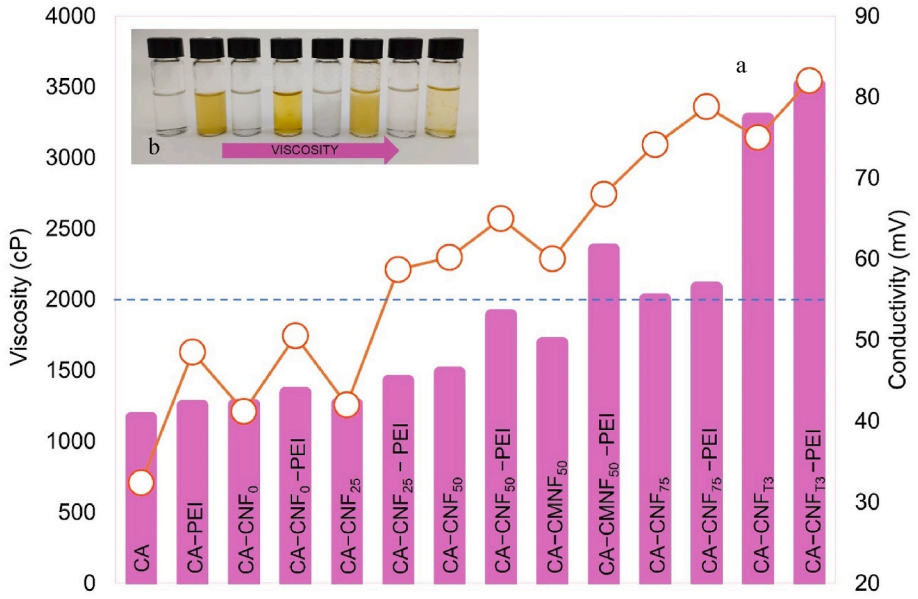

Fig. 1. a) Viscosity and conductivity of all electrospinning solutions and b) visual aspect corresponding to CA, CA−PEI, CA−CNF_{50}, CA−CNF_{50}−PEI, CA−$CMNF_{50}$, CA−$CMNF_{50}$−PEI, CA−CNF_{T3}, and CA−CNF_{T3}−PEI, respectively.

Table 2
Physicomechanical characterization data for membranes.

Sample	Thickness (μm)	Density (g/cm^3)	Void Volume (%)	Gurley porosity (s) With micropores	Tensile Index (Nm/g)	Elongation (%)	Mullen Index (kPa•m^2/g)
CA	71.00 ± 0.1	0.70 ± 0.02	45.67	2.08 ± 0.01	5.02 ± 0.26	2.52 ± 0.20	0.98 ± 0.01
CA−PEI	73.33 ± 0.3	0.68 ± 0.01	47.12	1.63 ± 0.05	13.47 ± 1.62	1.08 ± 0.15	1.07 ± 0.05
CA−CNF_0	75.00 ± 0.3	0.49 ± 0.01	61.52	1.85 ± 0.10	14.22 ± 0.89	1.44 ± 0.27	1.04 ± 0.09
CA−CNF_0−PEI	72.33 ± 0.1	0.46 ± 0.01	63.69	2.85 ± 0.06	17.68 ± 2.10	5.08 ± 0.31	0.79 ± 0.03
CA−CNF_{25}	68.67 ± 0.6	0.62 ± 0.05	51.91	7.36 ± 0.02	18.70 ± 1.43	3.14 ± 0.66	0.86 ± 0.03
CA−CNF_{25} – PEI	74.00 ± 0.3	0.61 ± 0.01	52.64	3.13 ± 0.01	18.15 ± 1.12	3.48 ± 0.55	0.80 ± 0.01
CA−CNF_{50}	74.02 ± 0.1	0.80 ± 0.01	37.43	5.33 ± 0.06	19.89 ± 1.18	2.31 ± 0.42	1.24 ± 0.08
CA−CNF_{50} −PEI	65.33 ± 0.5	0.77 ± 0.03	39.62	2.31 ± 0.09	20.06 ± 0.77	3.68 ± 0.30	0.61 ± 0.01
CA−CNF_{75}	72.13 ± 0.1	0.82 ± 0.01	36.22	3.86 ± 0.02	26.94 ± 0.74	4.00 ± 0.25	2.77 ± 0.12
CA−CNF_{75} − 6 wt% PEI	76.00 ± 0.1	0.61 ± 0.01	52.68	2.28 ± 0.02	18.63 ± 1.25	5.31 ± 0.54	2.88 ± 0.03
CA−CNF_{75} − 5 wt% PEI	86.30 ± 0.5	0.70 ± 0.05	45.65	3.53 ± 0.03	23.33 ± 0.25	3.12 ± 0.41	2.38 ± 0.02
CA−CNF_{75} − 4 wt% PEI	86.71 ± 0.2	0.70 ± 0.02	45.52	4.12 ± 0.02	26.26 ± 1.44	5.62 ± 1.92	2.29 ± 0.17
CA−CNF_{75} − 3 wt% PEI	88.33 ± 0.1	0.80 ± 0.05	37.87	3.82 ± 0.70	24.22 ± 0.55	3.39 ± 0.04	2.04 ± 0.06
CA−CNF_{75} − 2 wt% PEI	88.28 ± 0.3	0.81 ± 0.02	36.98	3.66 ± 0.03	24.75 ± 1.27	3.79 ± 0.15	2.05 ± 0.11

density; combining these CNF with PEI further decreased it. In contrast, membranes with pretreated CNF, obtained using oxalic acid at different concentrations, exhibited a substantial increase in density compared to those with CNF without pretreatment. The membranes with the highest concentration of pretreated CNF showed the greatest increase in density, while the addition of PEI to these membranes generally resulted in a slight reduction. The highest density was observed in the membranes with CNF_{75}, indicating that the most intensive pretreatment leads to the most compact and integrated structure within the CA matrix. The impact of PEI on these pretreated membranes varied with concentration, but certain combinations, such as CNF_{75} with specific PEI concentrations, maintained high compactness, which could be beneficial for CO_2 capture applications. These findings suggest that pretreating CNF with oxalic acid enhances their integration into the CA matrix, leading to denser membranes.

The inclusion of PEI generally enhanced the void volume in all samples, whether composed of pure cellulose or mixed with CNF. Without PEI, the void volume was highest in samples without pretreatment and declined as the oxalic acid concentration in the pretreatment increased. As the amount of PEI increases, the void volume in the CA−CNF_{75} samples generally increases as well. The increase in porosity caused by PEI addition was likely due to repulsion between protonated moieties, considering that the pK_a of its secondary $-NH_2^+-$ groups is as high as 10.3 (estimated with Chemaxon's MarvinSketch). In this sense, the presence of PEI increased the median pore size (d_{50}) from 0.4 μm in CA-CNF_{75} to 1.1 μm in CA-CNF_{75}-PEI (Fig. S2).

Consistent with this, the resulting membranes exhibited high porosity but were inadequate to withstand the CO_2 pressure accumulated during adsorption tests. To ensure proper performance, micropores were introduced, reducing the Gurley value from over 450 s to below 8 s. The choice of pretreatment intensity and PEI concentration is crucial for optimizing the structural properties of CA membranes, particularly in enhancing their CO_2 capture efficiency.

The tensile index results aligned with those reported by Bastida et al. (2024). Nanofibers reinforced the CA membranes, increasing their tensile strength by over 520%. Specifically, increasing the oxalic acid

concentration in the pretreatment process leads to a corresponding rise in the tensile index, with the highest value achieved using CNF_{75}.

On one hand, the introduction of PEI into the CA membranes had either mixed or non-significant effects on tensile properties. A two-way ANOVA test did not allow to reject the null hypothesis (*i.e.*, no significant influence), since the p-value was 0.27. On the other hand, the burst index increased with the addition of nanofibers, but it consistently decreased when PEI was introduced.

Regardless of the mechanical properties, the electrospinning process was successfully achieved, as depicted in the micrographs of Fig. 2. An overall homogeneity is observed in the filaments. Nevertheless, the introduction of PEI into the system leads to the formation of sheared filaments and clusters. The same behavior is observed with the addition of CNF and intensifies with the strength of the pretreatment carried out. Secondary filaments are formed and the factors that cause this disparity are related to the viscosity and conductivity of the polymeric dispersion (Hou et al., 2016). The highly charged PEI polymer and CNF promotes an increase in charge density in the ejected polymer jet, creating a repulsive force in the jet greater than the surface tension of the jet solution when passing through an electric field. The repulsive force splits into filaments of different sizes as it moves toward the collector (Jiang et al., 2023).

It was also observed that the nature of the CNF used strongly influences the density of the membranes. The oxalic acid pretreatment generated more closed membranes and lower porosity, in terms of reduced free volume and smaller pore size. For instance, d_{50} was 1.5 μm for CA-CNF_0 and 0.4 μm for CA-CNF_{75} (Fig. S2). This was expected, due to the greater viscosity, electrical charge and smaller size of the CNF that modify the flow. CNF fill the pores, creating a more compact material, but their accommodation and interaction depend largely on their intrinsic properties.

The microstructures of the post-wash membranes containing PEI are shown in Fig. 3, revealing the collapse of the structures. The phenomenon observed in the microscopy after being washed can be attributed to several factors. The NaOH solution can cause partial hydrolysis of cellulose acetate, converting some regions into more hydrophilic cellulose (Greish et al., 2010). This change increases the swelling of the filaments when rinsed with water, leading to a compacted structure. In addition, differential swelling rates of the membrane components in water, especially after NaOH treatment, can create internal stresses that compact the structure. Surface tension during drying can further contribute to filaments compaction. Residual water attraction can induce filament adhesion, particularly under conditions of uneven or rapid drying, resulting in increased capillary forces that generate additional stresses and consequently compact the filaments. Despite enhancements of membrane performance by washing were neither expected nor attained, the resulting materials can be deemed apter for repeated use in the treatment of streams with high partial pressures of water vapor, with condensed water, and even with alkaline gases such as ammonia.

3.3. Adsorption of CO_2

First, it is worth noting that the presence of PEI, intrinsically alkaline (pK_a ~10.3), grants the quantitative deprotonation of CNF's carboxyl groups (pK_a < 3.7) (McDonagh and Chinga-Carrasco, 2020). In this exchange, PEI is in turn protonated. Ionic interactions are anchoring points that get complemented by OH…NH dipole-dipole interactions and OH…NH_2^+ ion-dipole interactions.

The adsorption mechanism is governed by the interaction of CNF-anchored PEI with CO_2 through the ammonium carbonate/bicarbonate pathway (Fig. 4). As for the CO_2 adsorption process at the initial stage, it mainly arises from the formation of carbamates or bicarbonate species between CO_2 and amino groups. After the superficial amino sites

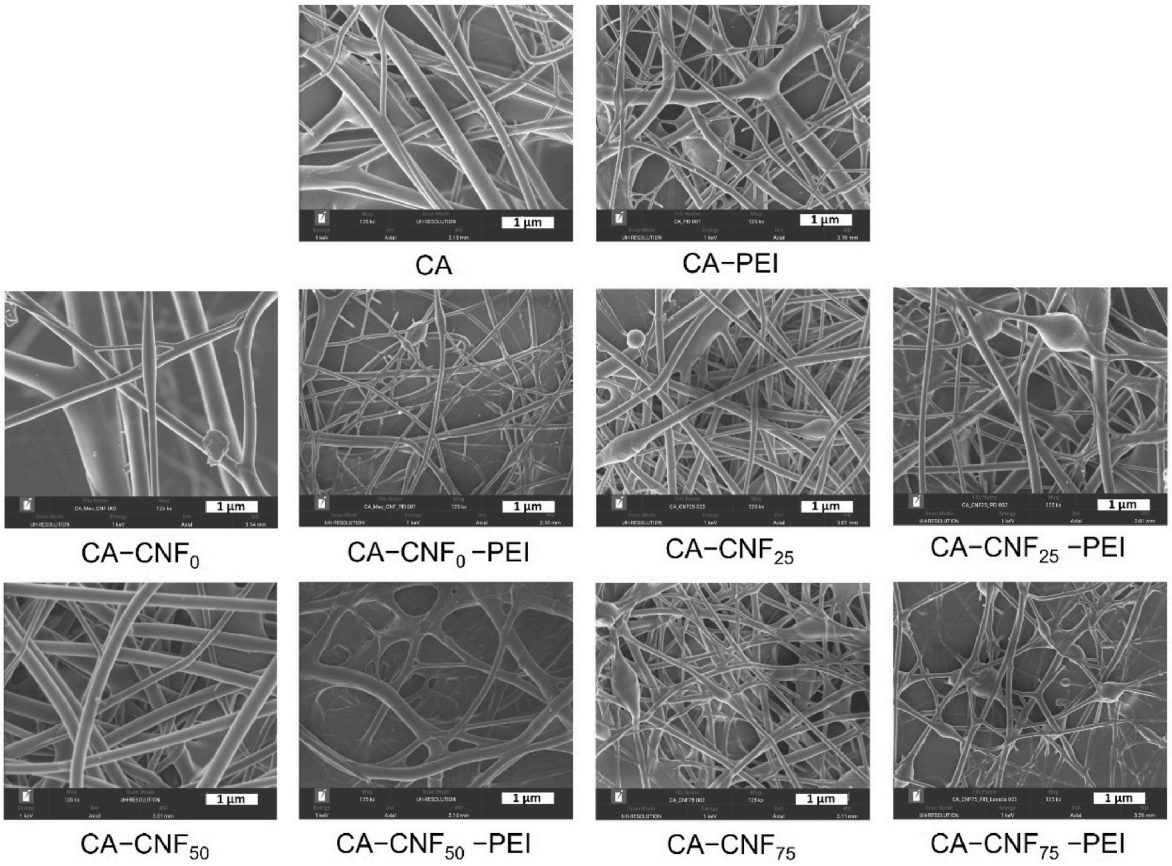

Fig. 2. SEM images of the different membranes.

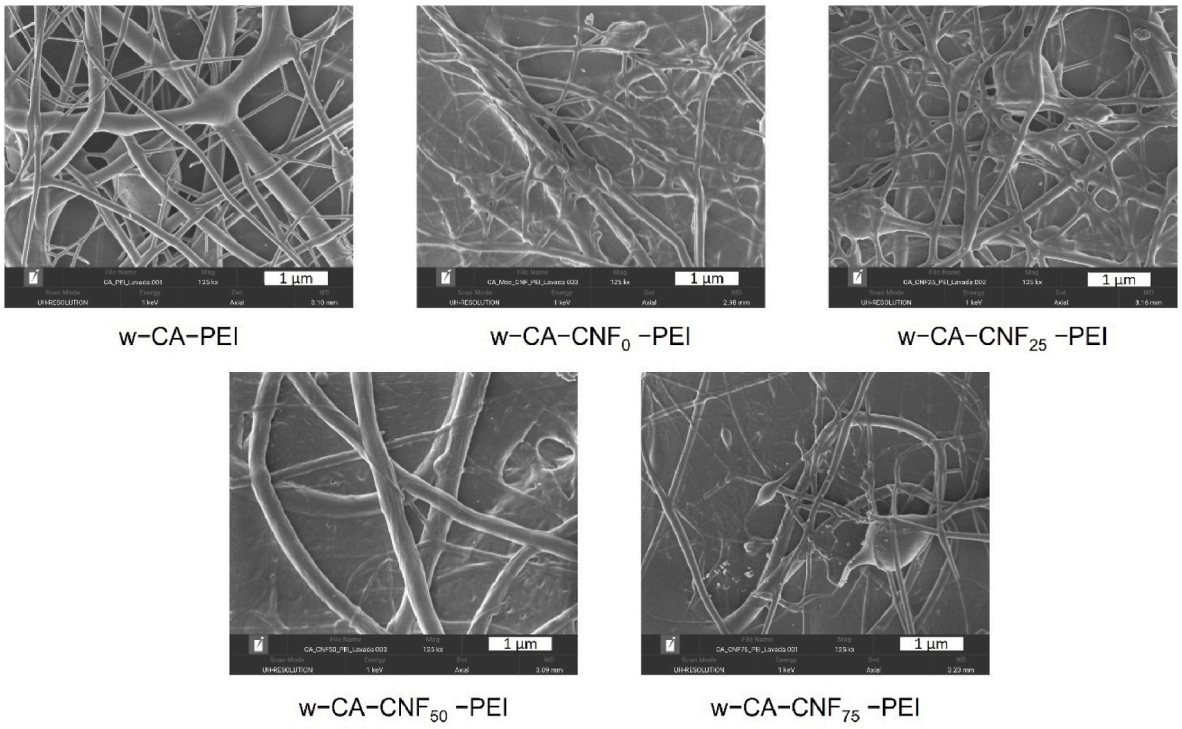

Fig. 3. SEM images of the different washed membranes.

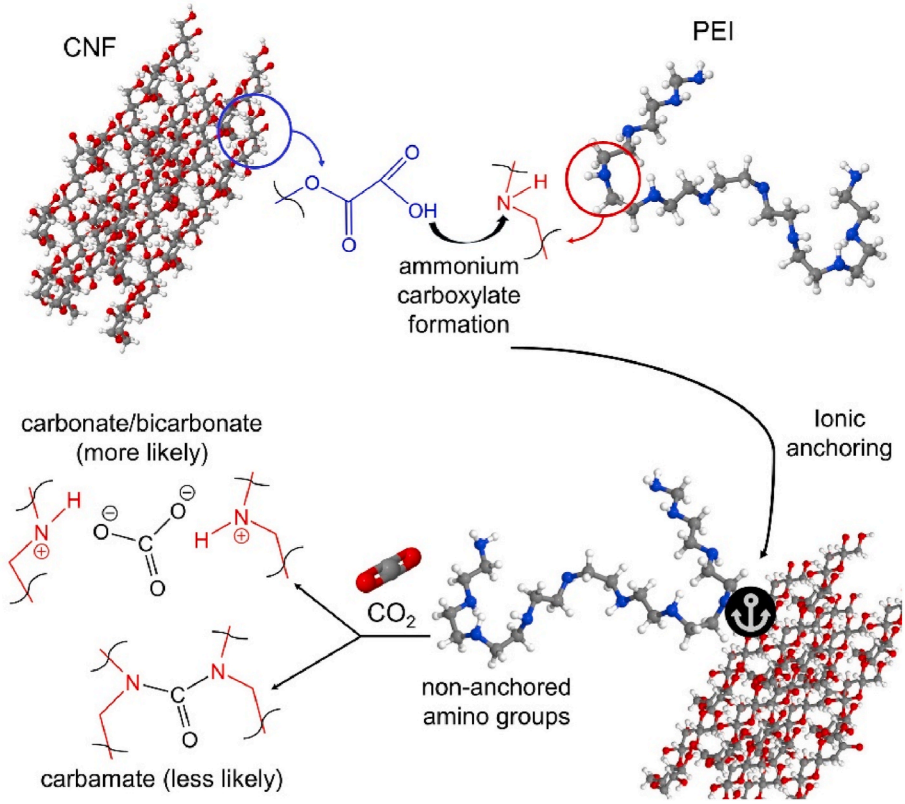

Fig. 4. PEI's interaction mechanism with acidic species and CO_2 through ammonium carbonate/bicarbonate pathway.

were completed occupied, CO_2 continued to be adsorbed with a lower adsorption rate as a result of the internal diffusion resistance through the filaments. One of the major bottlenecks for deliverable CO_2 adsorbents is the slow adsorption kinetics.

The adsorption rate of all membranes is shown in Fig. 5, and to enhance understanding, the results will be discussed by distinguishing in different groups. On the one hand, CA membranes, as well as the washed and unwashed CA−PEI membranes, showed a slow adsorption rate,

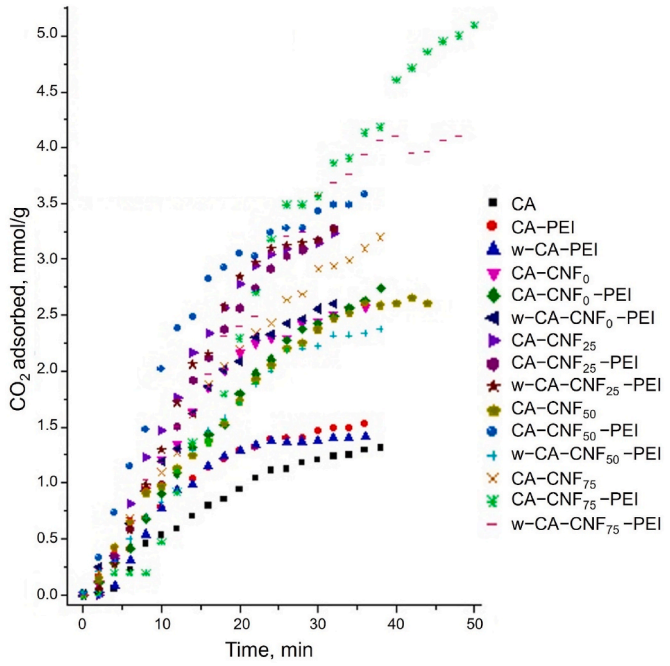

Fig. 5. CO_2 adsorption kinetics of all membranes, at 25 °C.

reaching saturation after approximately 20 min. CA membranes exhibit a deficient CO_2 uptake. This behavior is governed by a physisorption process and is further hindered by the low interaction energy between CO_2 molecules and the membrane surface. The addition of PEI shows a slight beneficial effect, though there is still potential for further enhancement. On the other hand, integrating CNF introduces a synergistic effect that enhances the overall performance. All membranes containing 6 wt% CNF show enhanced capture capacity. However, most of this capacity is lost after washing, as the low content of carboxyl groups is insufficient to retain the PEI, leading to its elution from the membranes. Regarding the kinetics, the first stage is faster, and saturation is reached at longer times compared to the previous cases. Specifically, CA−CNF_{25} membrane demonstrate superior performance compared to others, including some containing PEI. This can be attributed to the high membrane's porosity. Successfully, on the top of the graph, it is seen that CNF_{50} and CNF_{75} achieve the highest retention capacities. Focusing our analysis on the membranes containing the nanofibers with the most intense pretreatment, we find that they exhibit the fastest kinetics and require the longest time to reach saturation. These findings suggest that membrane performance is directly related to the properties of CNF, making them ideal candidates for this application.

The adsorption capacity values found are in line with the findings of other investigations. Lin et al. (2013) obtained a CO_2 adsorption capacity in their metal-organic adsorbent with PEI of 4.2 mmol/g in the first 5 min, and subsequently, the sample was completely saturated. Pore blocking and PEI droplet formation can, in principle, decrease the CO_2 sorption capacity and diffusivity in the solid sorbent. Besides, a PEI-grafted polypropylene containing 83 wt% of PEI was found to exhibit a maximum adsorption capacity of 5.91 mmol/g at 25 °C (Wu et al., 2014). In turn, a cellulose-based aerogel containing epoxy-modified PEI had a maximum adsorption capacity of 6.45 mmol/g at 25 °C under pure dry CO_2 (Chen et al., 2023). These and other strategies are summarized in Table 3. Nonetheless, any comparison should be made with caution, considering the different aforementioned conditions such as pressure and gas composition.

Al-Marri et al. (2017), in their study on the CO_2 adsorption/desorption kinetics of PEI mesoporous silicas, state that based on the nitrogen content in PEI, and assuming that all primary and secondary nitrogen atoms are active for CO_2 adsorption, maximum sorption capacities can be predicted to be between 16.7 and 12.5 mmol/g of material. However, these values have never been achieved under ambient pressure. The researchers suggest a potential explanation: PEI blocks pores and microchannels, forms a skin, and limits access and exposure to CO_2.

Table 3
CO_2 adsorption capacity of different PEI-containing materials reported in the literature.

Approach	Capacity (mmol/g)	Reference
Metal-organic framework with PEI	4.2	Lin et al. (2013)
PEI-grafted polypropylene	5.91	Wu et al. (2014)
PEI-functionalized porous chitosan beads	3.6	Fujiki and Yogo (2014)
Polyamide/carbon nanotube impregnated with PEI	1.2	Zainab et al. (2017)
Cellulose aerogel with epoxy-functionalized PEI	6.45	Chen et al. (2023)
w−CA−CNF_{75} −PEI	4.96	This work

Therefore, we may be experiencing similar limitations due to the deposition of PEI inside and outside the pores in the form of liquid droplets, suggesting the need to optimize the distribution and amount of PEI in our membranes to improve their CO_2 capture performance.

The chemical composition of membranes surface was investigated using EDS, and the results are listed in Table 4.

As expected, all membranes contain carbon and oxygen. In addition, membranes with PEI contain nitrogen atoms of the amine group. When PEI was added to CA, the lateral polar groups between the NH group of PEI, and the OH^- group of CA exhibit a repulsive force due to the electrical force that causes PEI to diffuse outward to the CA fiber surface (Hou et al., 2016). Nevertheless, when the membrane is flushed with NaOH and water, PEI content is completely lost. It should be attributed to the PEI content being physically adsorbed on the individual filament surfaces.

The incorporation of CNF is expected to enhance the retention of PEI on the membrane surface, ensuring its availability for CO_2 capture, which is the primary objective of this study. However, despite achieving higher N rates in the membranes, the N content decreases in all cases after flushing, indicating that not all PEI remains bound. Membranes with CNF pretreated more intensively with oxalic acid retained the most

Table 4
Elemental Analysis: References and membranes with 6 wt% of PEI and different CNF (6 wt%), with and without washing.

Sample	Carbon	Oxygen	Nitrogen	Others (wt %)[a]
	Mass Norm. (wt%)	Mass Norm. (wt%)	Mass Norm. (wt%)	
CA	59.54	40.46	0.00	0.00
CA−PEI	59.30	39.69	1.00	0.01
w−CA−PEI	59.53	40.47	0.00	0.00
CA−CNF_0	59.40	39.87	0.00	0.73
CA−CNF_0 −PEI	59.86	37.85	2.29	0.00
w−CA−CNF_0 −PEI	59.60	40.07	0.33	0.00
CA−CNF_{25}	60.22	39.65	0.00	0.13
CA−CNF_{25} −PEI	60.03	37.23	2.74	0.00
w−CA−CNF_{25} −PEI	62.42	37.55	0.00	0.03
CA−CNF_{50}	59.48	40.52	0.00	0.00
CA−CNF_{50} −PEI	60.80	34.43	4.77	0.00
w−CA−CNF_{50} −PEI	59.77	35.34	4.53	0.36
CA−CNF_{75}	60.66	39.34	0.00	0.00
CA−CNF_{75} −PEI	57.37	37.14	5.48	0.01
w−CA−CNF_{75} −PEI	58.73	34.88	5.33	1.06

[a] Elements such as Na remaining from the washing stage or other environmental contaminants.

PEI after washing. At the magnification levels in Fig. 2, all electrospun filaments apparently have smooth and uniform surfaces. However, Fig. 3 reveals that the surface is not even and has become mostly roughened, particularly for CA−CNF_{50} −PEI. This is due to the removal of PEI, which creates certain spaces and pores on filaments surface. Hence, arrangement and interactions of $–COO^-$ groups (CNF) with $–NH_2^+–$ groups (PEI), along with the resulting morphology of the membrane, are significant factors to consider.

Besides, mapping reveals a significant number of pearl-like aggregates in the presence of PEI, which are not observed in its absence (Fig. 6). After rinsing the membranes, these aggregates are significantly reduced in the CA−PEI membrane. However, they remain largely intact when CNF are present in the system. This behavior is particularly evident in the case of CA−CNF_{75} −PEI, attributed to the stronger synergistic interaction achieved between all membrane components.

The elution of PEI from the membranes during washing indicates that we are using it in excess. To optimize the PEI content without compromising CO_2 capture capacity, we will analyze membranes containing 6 wt% CNF_{75} with varying PEI contents of 2, 3, 4, 5, and 6 wt%.

Fig. 7 illustrates the CO_2 capture capacity of membranes containing 6 wt% CNF_{75} with different concentrations of PEI ranging from 2 to 6 wt %. The findings reveal that the capacity of the membranes to adsorb CO_2 rises when the PEI content increases. It should be noted that by adding 4 and 5 wt% of PEI, an adsorption greater than that achieved with 6 wt% was observed, with no significant differences between the two. These results indicate that 4 wt% is the optimal content to maximize the membranes potential. Beyond this amount, adsorption capability decreases slightly. This behavior could be related to the dispersion of PEI within the filaments. When all mesopore channels are filled, PEI primarily could mainly cover the outer surface of the structures and disperse into macropores, eventually covering the entire surface. As a result, CO_2 could exclusivity react with the exposed PEI until it diffuses inward (Guo et al., 2017).

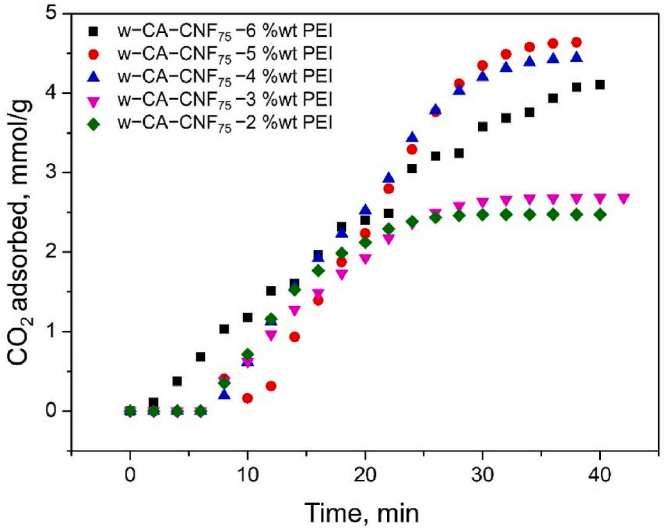

Fig. 7. CO_2 capture capacity for membranes containing 6 wt% CNF_{75} with different PEI contents of 2, 3, 4, 5, and 6 wt%, at 25 °C.

3.4. Modeling of adsorption kinetics

The rate of adsorption displayed a lag phase and then tended to asymptotic, equilibrium values. Whether the trend is hyperbolic, exponential, or logarithmic is a fruitful matter of discussion. To address this question, Eqs. (2)–(4) adapt the typical Lagrengen (or pseudo-first order), pseudo-second order, and Elovich integrated rate equations for adsorption (Aguado et al., 2021; Aniagor and Menkiti, 2018; Chan et al., 2024), respectively:

$$q(t) = q_e\left[1 - e^{k(t_0 - t)}\right] \quad \forall\ t \geq t_0 \tag{2}$$

$$q(t) = \frac{q_e^{\,2}\, k\,(t - t_0)}{1 + k\,(t - t_0)\, q_e} \quad \forall\ t \geq t_0 \tag{3}$$

$$q(t) = \frac{1}{\beta}\ln[\alpha(t - t_0) + 1] \quad \forall\ t \geq t_0 \cap q < q_e \tag{4}$$

where q is the extent of adsorption (mmol CO_2/g), q_e is the extent of adsorption at equilibrium (saturated membrane), t_0 is the lag time, k is

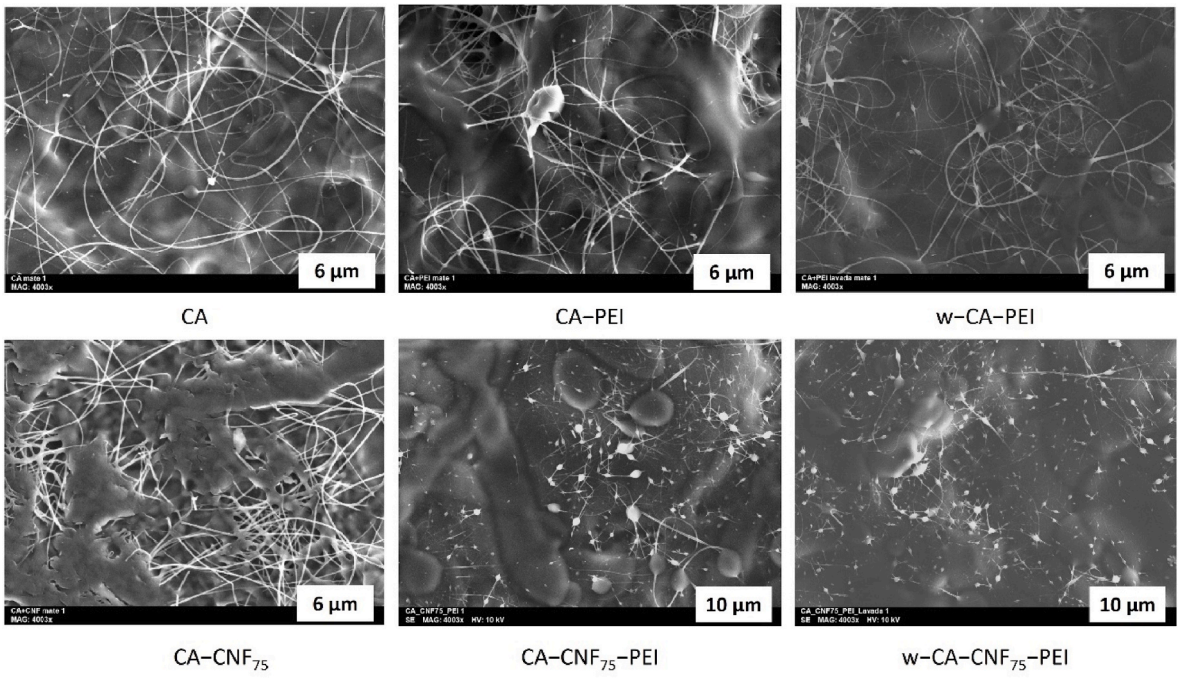

Fig. 6. Sem images from Elemental analysis mapping.

the rate constant, α is the initial adsorption rate in the Elovich model, and β is a constant related to surface coverage. It should be noted that Eq. (4) can only be applied before q approaches q_e. To have q_e estimated, data were first fitted to Eqs. (2) and (3) (Table 5).

Lagrengen kinetics (Eq. (2)) generally described better the adsorption rate than Eq. (3), plausibly indicating that physisorption prevailed over chemisorption. Haga clic o pulse aquí para escribir texto. Furthermore, q_e was notably overestimated by the pseudo-second order model. For instance, the last six experimental values for w−CA−CNF_{75} −3 wt% PEI were 2.7 mmol/g, but the q_e value as estimated from Eq. (3) was as high as 3.9 mmol/g (Table 5).

Even though Elovich kinetics (Eq. (4)) have satisfactorily described the rate of CO_2 adsorption onto different materials (Borhan and Yusuf, 2020; Fatima et al., 2023), this was not the case of PEI-containing membranes. As can be seen from Table S2, R^2 lied below 0.90 in four cases. While fitting parameters were acceptable in all cases without PEI, the global applicability of pseudo-first order kinetics (successfully describing all membranes) makes it the best choice for adsorption rate modeling.

3.5. Infrared spectra

The FTIR spectra for CA, CA−PEI, CA−CNF_{75}, and CA−CNF_{75} −6 wt % PEI are shown in Fig. 8a. The broad band between 3660 and 3330 cm^{-1} in CA corresponds to O–H stretching. The characteristic peak within the 3050–2760 cm^{-1} band corresponds to C–H vibrations. Absorption bands are observed at 1731 cm^{-1} for the carbonyl group (C=O stretching), and at 1435 and 1360 cm^{-1} from C–H bending. Strong absorption bands at 1218 cm^{-1} and 1025 cm^{-1} are assigned to C–O stretching in the acetyl group and in the backbone's C–O–C bonds, respectively (Araújo et al., 2020; Chen et al., 2018). When CNF are present in the membrane, a unique peak emerges at 1670 cm^{-1}, attributed to the $–COO^-$ groups from the oxalic acid pretreatment, slightly shifted (Bastida et al., 2022). With PEI inclusion, the peak at 3480 cm^{-1} becomes more intense due to hydrogen bonding between (–NH–) in PEI and –OH in CA (Yoon et al., 2024). Additionally, the ~2920 cm^{-1} peak intensifies, likely due to overlap with the 2838 cm^{-1} signal from N–H stretching vibrations (Xian et al., 2015). Likewise, the band at 780 cm^{-1} corresponds to C–NH wagging (Zhao et al., 2021). Besides, the N–H asymmetric bending vibration is discernible at 1570 cm^{-1} (Lin et al., 2013), confirming successful PEI loading onto the membranes. Fig. 8b compares the pre- and post-adsorption states of the membrane with the highest CO_2 adsorption performance. After adsorption, the peak at 3300 cm^{-1} tends to disappear and it suggests that CO_2 may be interacting with

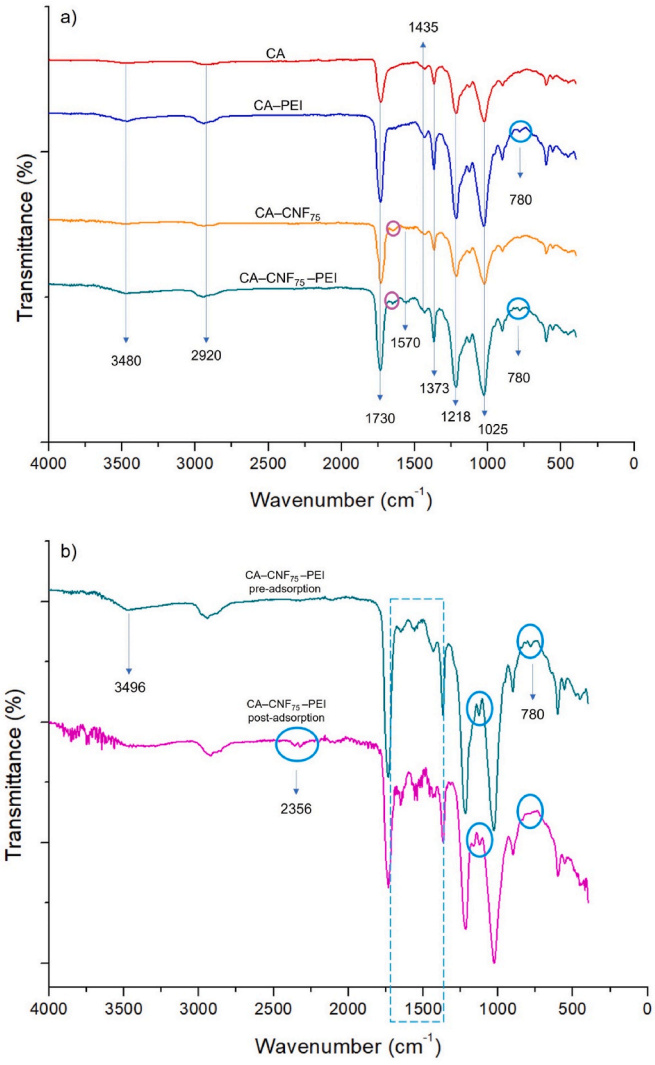

Fig. 8. FTIR spectra a) analyzing the CNF and PEI effect and b) comparison between pre- and post-adsorption states of the membrane with the highest CO_2 adsorption performance.

Table 5
Fitting parameters of Lagrengen and pseudo-second order rate equations (Eqs. (2) and (3)).

Sample	*Lagrengen kinetics*				*Pseudo-second order kinetics*			
	t_0 (min)	q_e (mmol/g)	k (min^{-1})	R^2	t_0 (min)	q_e (mmol/g)	k (g $mmol^{-1}$ min^{-1})	R^2
CA	2.0	1.58	0.051	0.991	2.6	2.24	0.0187	0.989
CA−PEI	1.9	1.60	0.086	0.995	3.3	1.98	0.0533	0.993
w−CA−PEI	4.7	1.43	0.143	0.992	5.9	1.66	0.1296	0.983
CA−CNF_0	3.6	2.72	0.090	0.993	4.5	3.42	0.0295	0.990
CA−CNF_0 −PEI	3.2	3.59	0.041	0.993	3.5	5.37	0.0057	0.993
w−CA−CNF_0 −PEI	3.2	2.97	0.074	0.992	3.9	4.00	0.0172	0.990
CA−CNF_{25}	3.7	3.53	0.091	0.992	4.4	4.60	0.0198	0.985
CA−CNF_{25} −PEI	4.7	3.84	0.072	0.993	5.1	5.43	0.0109	0.985
w−CA−CNF_{25} −PEI	4.9	3.59	0.095	0.994	5.4	4.75	0.0191	0.980
CA−CNF_{50}	1.8	3.29	0.043	0.992	2.2	4.76	0.0070	0.978
CA−CNF_{50} −PEI	2.8	3.59	0.111	0.990	4.8	4.18	0.0413	0.991
w−CA−CNF_{50} −PEI	4.0	2.72	0.065	0.987	4.6	3.71	0.0157	0.988
CA−CNF_{75}	2.6	3.99	0.045	0.985	3.1	5.77	0.0062	0.994
CA−CNF_{75} −6 wt% PEI	8.8	5.70	0.055	0.981	8.9	6.89	0.0094	0.953
w−CA−CNF_{75} −6 wt% PEI	3.6	4.96	0.038	0.990	5.2	6.21	0.0070	0.970
w−CA−CNF_{75} −5 wt% PEI	9.4	5.31	0.061	0.987	9.3	6.40	0.0100	0.880
w−CA−CNF_{75} −4 wt% PEI	8.0	5.20	0.059	0.985	8.4	6.32	0.0106	0.962
w−CA−CNF_{75} −3 wt% PEI	7.0	2.95	0.086	0.981	7.2	3.91	0.0200	0.976
w−CA−CNF_{75} −2 wt% PEI	7.2	2.57	0.136	0.985	7.5	3.14	0.0485	0.975

surface OH. Interestingly, new peaks appear in the post-adsorption membranes, around 2356 cm^{-1}, corresponding to the physiosorbed CO_2 (Stevens et al., 2008). Therefore, in the region between 1730 and 1370 cm^{-1} (dashed lines), variations in absorption are observed. This may be due to the formation of bridged bidentate carbonate bands at 1688 and 1361 cm^{-1}, and another band at 1623 cm^{-1}. Rege and Yang (2001) assigned the bands at 3605, 1640, 1480, and 1235 cm^{-1} to the surface reaction of CO_2 with hydroxyl groups forming bicarbonates on the surface. In addition, the peak at 780 cm^{-1}, which corresponds to C–NH wagging, disappeared. Fig. S3 presents the FTIR spectra for all membranes.

3.6. Reusability of membranes

In practical applications, it is important for the membranes to display stable performance during cyclical operation. For this reason, several adsorptions–desorption cycles were carried out. As aforementioned, the CO_2 adsorption mechanism involves both physisorption and, to a lesser extent, chemisorption. To ensure the complete remotion of CO_2 after each adsorption cycle, thermal desorption (80 °C), which suffices to remove CO_2 attached by weak intermolecular forces, was preceded by alkaline washing. This step causes the desorption and elution of all carbonate species.

Fig. 9 displays the CO_2 adsorption capacities for five successive cycles. The multiple consecutive tests suggested that the original capacity is slightly reduced in the fourth cycle.

This adsorption capacity is unchanged during the following cycle so that a stable condition is attained. Carbon dioxide adsorption–desorption can be carried out in successive cycles, without significant loss of properties. This behavior is similar to that reported by Sanz et al. (2010) for their mesoporous silica materials impregnated with PEI. The deviations observed in the adsorption values across different cycles lie within the margin of experimental error, indicating that there are no significant differences between them.

4. Conclusions

The functionalization of CA membranes for CO_2 adsorption was successfully achieved by incorporating different CNF that interact with PEI and retain it within the membrane. This study revealed that CNF_{T3} and CMNF were not suitable for spinning, due to the high thickening effect of the former and the needle obstruction produced by the latter. Nevertheless, membranes were effectively produced with 6 wt% of oxalic acid-treated CNF, in such way that the chemical pretreatment directly impacted the adsorption capability of the membranes.

More intense oxalic acid treatment resulted in more carboxylate groups on CNF, allowing for more PEI retention and ultimately leading to CO_2 adsorption exceeding 4 mmol CO_2/g. Besides, it was found that PEI partially elutes during membrane washing. For CA–CNF_{75}–PEI membranes, the optimum percentage of PEI for maximizing adsorption while avoiding elution to aqueous systems is 4 wt%. Not less importantly, membranes withstood at least five adsorption-desorption cycles with no significant loss of performance.

CRediT authorship contribution statement

Gabriela A. Bastida: Writing – original draft, Software, Methodology, Investigation, Formal analysis, Data curation. **Roberto J. Aguado:** Writing – review & editing, Writing – original draft, Validation, Software, Data curation. **Marc Delgado-Aguilar:** Visualization, Validation, Resources, Formal analysis. **Miguel A. Zanuttini:** Validation, Supervision, Resources, Conceptualization. **María V. Galván:** Visualization, Supervision, Methodology, Formal analysis. **Quim Tarrés:** Writing – review & editing, Visualization, Validation, Supervision, Resources, Methodology, Investigation.

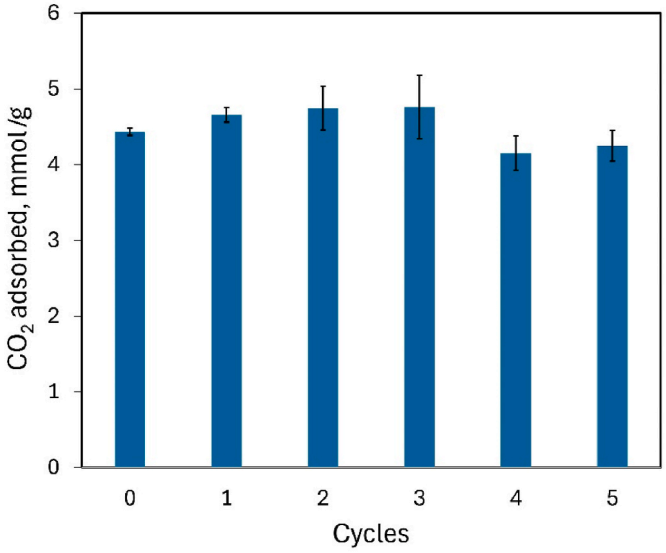

Fig. 9. Lifetime: adsorption-desorption cycles for CA−CNF_{75} −4 wt% PEI.

Declaration of competing interest

The authors declare that they have no known competing financial interests or personal relationships that could have appeared to influence the work reported in this paper.

Acknowledgments

The authors wish to acknowledge the financial support of the Spanish Ministry of Science, Innovation and Universities to the project NBEA (PID2023-147456OB-C21). Marc Delgado-Aguilar and Quim Tarrés are Serra Húnter Fellows.

Appendix A. Supplementary data

Supplementary data to this article can be found online at https://doi.org/10.1016/j.jclepro.2024.144428.

Data availability

Data will be made available on request.

References

Aguado, R., Murtinho, D., Valente, A.J.M., 2021. Association of antioxidant monophenolic compounds with β-cyclodextrin-functionalized cellulose and starch substrates. Carbohydr. Polym. 267. https://doi.org/10.1016/j.carbpol.2021.118189.

Al-Marri, M.J., Kuti, Y.O., Khraisheh, M., Kumar, A., Khader, M.M., 2017. Kinetics of CO2 adsorption/desorption of polyethyleneimine-mesoporous silica. Chem. Eng. Technol. 40, 1802–1809. https://doi.org/10.1002/ceat.201600452.

Aniagor, C.O., Menkiti, M.C., 2018. Kinetics and mechanistic description of adsorptive uptake of crystal violet dye by lignified elephant grass complexed isolate. J. Environ. Chem. Eng. 6, 2105–2118. https://doi.org/10.1016/j.jece.2018.01.070.

Araújo, D., Castro, M.C.R., Figueiredo, A., Vilarinho, M., Machado, A., 2020. Green synthesis of cellulose acetate from corncob: physicochemical properties and assessment of environmental impacts. J. Clean. Prod. 260, 120865. https://doi.org/10.1016/j.jclepro.2020.120865.

Bastida, G.A., Aguado, R.J., Galván, M.V., Zanuttini, M., Delgado-Aguilar, M., Tarrés, Q., 2024. Impact of cellulose nanofibers on cellulose acetate membrane performance. Cellulose 31, 2221–2238. https://doi.org/10.1007/s10570-024-05760-9.

Bastida, G.A., Schnell, C.N., Mocchiutti, P., Solier, Y.N., Inalbon, M.C., Zanuttini, M.Á., Galván, M.V., 2022. Effect of oxalic acid concentration and different mechanical pretreatments on the production of cellulose micro/nanofibers. Nanomaterials 12. https://doi.org/10.3390/nano12172908.

Borhan, A., Yusuf, S., 2020. Activation of rubber-seed shell waste by malic acid as potential CO2 removal: isotherm and kinetics studies. Materials 13, 1–20. https://doi.org/10.3390/ma13214970.

Chan, A.A., Abdul Raman, A.A., Chong, W.L., Buthiyappan, A., 2024. Graphene oxide impregnated activated carbon derived from coconut shell through hydrothermal carbonization for cationic dye removal: adsorptive performance, kinetics, and chemistry of interaction. J. Clean. Prod. 437, 140655. https://doi.org/10.1016/j.jclepro.2024.140655.

Chauhan, D., Solanki, P.R., 2019. Hydrophilic and insoluble electrospun cellulose acetate fiber-based biosensing platform for 25-hydroxy vitamin-D3Detection. ACS Appl. Polym. Mater. 1, 1613–1623. https://doi.org/10.1021/acsapm.9b00179.

Chen, W., Ma, H., Xing, B., 2020. Electrospinning of multifunctional cellulose acetate membrane and its adsorption properties for ionic dyes. Int. J. Biol. Macromol. 158, 1342–1351. https://doi.org/10.1016/j.ijbiomac.2020.04.249.

Chen, W., Zhang, L., Liu, C., Feng, X., Zhang, J., Guan, L., Mi, L., Cui, S., 2018. Electrospun flexible cellulose acetate-based separators for sodium-ion batteries with ultralong cycle stability and excellent wettability: the role of interface chemical groups. ACS Appl. Mater. Interfaces 10, 23883–23890. https://doi.org/10.1021/acsami.8b06706.

Chen, X., Lin, J., Wang, H., Yang, Y., Wang, C., Sun, Q., Shen, X., Li, Y., 2023. Epoxy-functionalized polyethyleneimine modified epichlorohydrin-cross-linked cellulose aerogel as adsorbents for carbon dioxide capture. Carbohydr. Polym. 302, 120389. https://doi.org/10.1016/j.carbpol.2022.120389.

Deitzel, J.M., Kleinmeyer, J., Harris, D., Tan, N.C.B., 2001. The effect of processing variables on the morphology of electrospun nanofibers and textiles. Polymer (Guildf) 42, 261–272.

Delgado-Aguilar, M., González, I., Tarrés, Q., Alcalà, M., Pèlach, M.À., Mutjé, P., 2015. Approaching a low-cost production of cellulose nanofibers for papermaking applications. Bioresources 10, 5345–5355.

Dos Santos, D.M., Correa, D.S., Medeiros, E.S., Oliveira, J.E., Mattoso, L.H.C., 2020. Advances in functional polymer nanofibers: from spinning fabrication techniques to recent biomedical applications. ACS Appl. Mater. Interfaces. https://doi.org/10.1021/acsami.0c12410.

Espinosa, E., Rol, F., Bras, J., Rodríguez, A., 2020. Use of multi-factorial analysis to determine the quality of cellulose nanofibers: effect of nanofibrillation treatment and residual lignin content. Cellulose 27, 10689–10705. https://doi.org/10.1007/s10570-020-03136-3.

Fatima, S.S., Borhan, A., Ayoub, M., Ghani, N.A., 2023. Modeling of CO2 adsorption on surface-functionalized rubber-seed shell activated carbon: isotherm and kinetic analysis. Processes 11. https://doi.org/10.3390/pr11102833.

Fujiki, J., Yogo, K., 2014. Carbon dioxide adsorption onto polyethylenimine-functionalized porous chitosan beads. Energy & Fuels 28, 6467–6474. https://doi.org/10.1021/ef500975g.

Greish, Y.E., Meetani, M.A., Al Matroushi, E.A., Shamsi, B. Al, 2010. Effects of thermal and chemical treatments on the structural stability of cellulose acetate nanofibers. Carbohydr. Polym. 82, 569–577. https://doi.org/10.1016/j.carbpol.2010.05.012.

Guo, X., Ding, L., Kanamori, K., Nakanishi, K., Yang, H., 2017. Functionalization of hierarchically porous silica monoliths with polyethyleneimine (PEI) for CO2 adsorption. Microporous Mesoporous Mater. 245, 51–57. https://doi.org/10.1016/j.micromeso.2017.02.076.

Hojat, N., Gentile, P., Ferreira, A.M., Šiller, L., 2023. Automatic pore size measurements from scanning electron microscopy images of porous scaffolds. J. Porous Mater. 30, 93–101. https://doi.org/10.1007/s10934-022-01309-y.

Hou, J.Z., Xue, H.L., Li, L.L., Dou, Y.L., Wu, Z.N., Zhang, P.P., 2016. Fabrication and morphology study of electrospun cellulose acetate/polyethylenimine nanofiber. Polym. Bull. 73, 2889–2906. https://doi.org/10.1007/s00289-016-1630-6.

Jang, M.-G., Yun, S., Kim, J.-K., 2022. Process design and economic analysis of membrane-integrated absorption processes for CO2 capture. J. Clean. Prod. 368, 133180. https://doi.org/10.1016/j.jclepro.2022.133180.

Jiang, S., Kang, Z., Liu, F., Fan, J., 2023. 2D and 3D electrospinning of nanofibrous structures by far-field jet writing. ACS Appl. Mater. Interfaces 15, 23777–23782. https://doi.org/10.1021/acsami.3c03145.

Li, S., Wang, X., Guo, Y., Hu, J., Lin, S., Tu, Y., Chen, L., Ni, Y., Huang, L., 2022. Recent advances on cellulose-based nanofiltration membranes and their applications in drinking water purification: a review. J. Clean. Prod. 333, 130171. https://doi.org/10.1016/j.jclepro.2021.130171.

Liao, J., Pham, K.A., Breedveld, V., 2021. TEMPO-CNF suspensions in the viscoelastic regime: capturing the effect of morphology and surface charge with a rheological parameter. Cellulose 28, 813–827. https://doi.org/10.1007/s10570-020-03572-1.

Lin, Y., Yan, Q., Kong, C., Chen, L., 2013. Polyethyleneimine incorporated metal-organic frameworks adsorbent for highly selective CO2 capture. Sci. Rep. 3. https://doi.org/10.1038/srep01859.

Liu, Q., Wang, X., Zhang, X., Ling, Z., Wu, W., Fu, X., Zhang, R., Hu, S., Li, X., Zhao, F., Bao, X., 2022. Polyethyleneimine-filled sepiolite nanorods-embedded poly(2,5-benzimidazole) composite membranes for wide-temperature PEMFCs. J. Clean. Prod. 359. https://doi.org/10.1016/j.jclepro.2022.131977.

Luo, D., Hu, S.Z., Huang, T., Zhang, N., Lei, Y.Z., Wang, Y., 2022. Electrospun cellulose acetate/polyethylenimine porous fibers toward highly efficient removal of Cr(VI). ACS Appl. Polym. Mater. https://doi.org/10.1021/acsapm.1c00836.

McDonagh, B.H., Chinga-Carrasco, G., 2020. Characterization of porous structures of cellulose nanofibrils loaded with salicylic acid. Polymers 12, 2538. https://doi.org/10.3390/polym12112538.

Meng, Y., Ju, T., Han, S., Gao, Y., Liu, J., Jiang, J., 2021. Exploring the stability on exposure to acid impurities of polyethyleneimine-functionalized silica for post-combustion CO2 capture. Chem. Eng. J. 421. https://doi.org/10.1016/j.cej.2020.127754.

Morais, M.S., Bonfim, D.P.F., Aguiar, M.L., Oliveira, W.P., 2022. Electrospun poly (vinyl alcohol) nanofibrous mat loaded with green propolis extract, chitosan and nystatin as an innovative wound dressing material. J Pharm Innov. https://doi.org/10.1007/s12247-022-09681-7.

Payne, M.E., Lou, Y., Zhang, X., Sahiner, N., Sandoval, N.R., Shantz, D.F., Grayson, S.M., 2020. Comparison of cross-linked branched and linear poly(ethylene imine) microgel microstructures and their impact in antimicrobial behavior, copper chelation, and carbon dioxide capture. ACS Appl. Polym. Mater. 2, 826–836. https://doi.org/10.1021/acsapm.9b01101.

Rege, S.U., Yang, R.T., 2001. A novel FTIR method for studying mixed gas adsorption at low concentrations: H 2 O and CO 2 on NaX zeolite and-alumina. Chem. Eng. Sci.

Sanz, R., Calleja, G., Arencibia, A., Sanz-Pérez, E.S., 2010. CO 2 adsorption on branched polyethyleneimine-impregnated mesoporous silica SBA-15. Appl. Surf. Sci. 256, 5323–5328. https://doi.org/10.1016/j.apsusc.2009.12.070.

Serra, A., González, I., Oliver-Ortega, H., Tarrès, Q., Delgado-Aguilar, M., Mutjé, P., 2017. Reducing the amount of catalyst in TEMPO-oxidized cellulose nanofibers: effect on properties and cost. Polymers 9. https://doi.org/10.3390/polym9110557.

Signori-Iamin, G., Santos, A.F., Mazega, A., Corazza, M.L., Aguado, R.J., Delgado-Aguilar, M., 2023. Bayesian-optimized random forest prediction of key properties of micro-/nanofibrillated cellulose from different woody and non-woody feedstocks. Ind. Crops Prod. 206, 117719. https://doi.org/10.1016/j.indcrop.2023.117719.

Stevens, R.W., Siriwardane, R.V., Logan, J., 2008. In situ fourier transform infrared (FTIR) investigation of CO2 adsorption onto zeolite materials. Energy Fuel. 22, 3070–3079. https://doi.org/10.1021/ef800209a.

Vakharia, V., Salim, W., Wu, D., Han, Y., Chen, Y., Zhao, L., Ho, W.S.W., 2018. Scale-up of amine-containing thin-film composite membranes for CO2 capture from flue gas. J Memb Sci 555, 379–387. https://doi.org/10.1016/j.memsci.2018.03.074.

Wu, Q., Chen, S., Liu, H., 2014. Effect of surface chemistry of polyethyleneimine-grafted polypropylene fiber on its CO2 adsorption. RSC Adv. 4, 27176–27183. https://doi.org/10.1039/c4ra01232a.

Xian, S., Xu, F., Ma, C., Wu, Y., Xia, Q., Wang, H., Li, Z., 2015. Vapor-enhanced CO2 adsorption mechanism of composite PEI@ZIF-8 modified by polyethyleneimine for CO2/N2 separation. Chem. Eng. J. 280, 363–369. https://doi.org/10.1016/j.cej.2015.06.042.

Xue, J., Wu, T., Dai, Y., Xia, Y., 2019. Electrospinning and electrospun nanofibers: methods, materials, and applications. Chem Rev. https://doi.org/10.1021/acs.chemrev.8b00593.

Yoon, J., Lee, J., Oh, S.G., 2024. Preparation of electrospun cellulose acetate/polyethylene imine bicomponent nanofibers for CO2 capture. Polym. Bull. 81, 1389–1401. https://doi.org/10.1007/s00289-023-04773-x.

Zainab, G., Iqbal, N., Babar, A.A., Huang, C., Wang, X., Yu, J., Ding, B., 2017. Free-standing, spider-web-like polyamide/carbon nanotube composite nanofibrous membrane impregnated with polyethyleneimine for CO2 capture. Compos. Commun. 6, 41–47. https://doi.org/10.1016/j.coco.2017.09.001.

Zhao, B., Kolibaba, T.J., Lazar, S., Grunlan, J.C., 2021. Environmentally-benign, water-based covalent polymer network for flame retardant cotton. Cellulose 28, 5855–5866. https://doi.org/10.1007/s10570-021-03874-y.